APPLIED PHYSICS

High–bit rate ultra-compact light routing with mode-selective on-chip nanoantennas

Rui Guo,[1] Manuel Decker,[1] Frank Setzpfandt,[2] Xin Gai,[3] Duk-Yong Choi,[3] Roman Kiselev,[4] Arkadi Chipouline,[5] Isabelle Staude,[1,2] Thomas Pertsch,[2] Dragomir N. Neshev,[1]* Yuri S. Kivshar[1]

Optical nanoantennas provide a promising pathway toward advanced manipulation of light waves, such as directional scattering, polarization conversion, and fluorescence enhancement. Although these functionalities were mainly studied for nanoantennas in free space or on homogeneous substrates, their integration with optical waveguides offers an important "wired" connection to other functional optical components. Taking advantage of the nanoantenna's versatility and unrivaled compactness, their imprinting onto optical waveguides would enable a marked enhancement of design freedom and integration density for optical on-chip devices. Several examples of this concept have been demonstrated recently. However, the important question of whether nanoantennas can fulfill functionalities for high-bit rate signal transmission without degradation, which is the core purpose of many integrated optical applications, has not yet been experimentally investigated. We introduce and investigate directional, polarization-selective, and mode-selective on-chip nanoantennas integrated with a silicon rib waveguide. We demonstrate that these nanoantennas can separate optical signals with different polarizations by coupling the different polarizations of light vertically to different waveguide modes propagating into opposite directions. As the central result of this work, we show the suitability of this concept for the control of optical signals with ASK (amplitude-shift keying) NRZ (nonreturn to zero) modulation [10 Gigabit/s (Gb/s)] without significant bit error rate impairments. Our results demonstrate that waveguide-integrated nanoantennas have the potential to be used as ultra-compact polarization-demultiplexing on-chip devices for high–bit rate telecommunication applications.

INTRODUCTION

Optical nanoantennas have the ability to establish efficient links between localized optical near fields and propagating light fields (1). They provide a promising pathway toward a range of advanced light manipulation capabilities, including directional scattering (2–4) and emission (5–7) of light, polarization conversion (8, 9), and plasmonic-assisted fluorescence enhancement (10–12). Although most research on optical nanoantennas has concentrated thus far on the interaction with free space propagating light waves, research targeting their use with guided-wave optics remains sparse. A promising avenue envisions functional plasmonic elements integrated with low-loss dielectric optical waveguides, aiming to create a fundamentally new link between electronic and photonic circuits (13, 14). Along these lines, several waveguide-integrated plasmonic structures were previously suggested, including plasmonic photodetectors (15–19), modulators (20, 21), and plasmonic amplifiers (22), but these did not take advantage of the possibilities offered by nanostructuring. Nanostructured optical antennas offer additional opportunities because of their resonant optical response, which can be tailored by geometry. They can enable extreme control of their scattering strength and directionality, depending on the properties of the exciting optical wave, such as frequency, polarization, and direction. This has been used in structured plasmonic film waveguides to selectively excite surface plasmons (23–28). Furthermore, excitation of localized modes of nanoantennas through low-loss waveguides and

controlled scattering into free space has been demonstrated in several previous works (29–33). This makes waveguide-integrated nanoantennas ideal candidates for ultra-compact optical couplers to mediate selective energy transfer between modes of different guided-wave structures, for example, from optical fibers (34) or free space (35) to on-chip integrated structures. First attempts to use nanoantennas as directional waveguide couplers have been explored recently (36–42). Their use can add a completely new dimension to the functionalities of on-chip devices and may ultimately increase the integration density and performance of photonic chips.

A question to answer for on-chip nanoantenna devices is to what extent complex functionalities can be realized on optical chips with control parameters and settings compatible to telecom data streams. In general, when designing optical couplers for signal manipulation, the aim is to uniquely connect a certain set of the eigenmodes in the exciting optical system with a defined subset of the modes in the target system to rout signals according to their spectral, spatial, or polarization properties. Ideally, there should be a one-to-one correspondence between the addressed modes in the exciting and the target system. For telecom applications, which mainly use single-mode waveguides, control parameters for routing are typically the wavelength and linear polarization of the signal modes, which have to be coupled to modes with specific propagation directions and polarization. Mode selectivity based on the wavelength of incident light was already demonstrated (42); however, the necessary difference between the usable wavelengths is very large due to the large bandwidths of the used antenna, making this control parameter impractical for telecom applications, which use closely spaced wavelength channels. Other demonstrations used a tunable array of several nanoantennas to couple a propagating waveguide mode to free-space modes with different propagation directions (37) or circularly polarized light for coupling to slab waveguides (38, 39). These approaches are not ideally suited for telecom applications because they

[1]Nonlinear Physics Centre and Centre for Ultrahigh-bandwidth Devices for Optical Systems, Research School of Physics and Engineering, Australian National University, Canberra, Australian Capital Territory 2601, Australia. [2]Institute of Applied Physics, Abbe Center of Photonics, Friedrich-Schiller-Universität Jena, D-07745 Jena, Germany. [3]Laser Physics Centre, Research School of Physics and Engineering, Australian National University, Canberra, Australian Capital Territory 2601, Australia. [4]Leibniz Institute of Photonic Technology, D-07745 Jena, Germany. [5]Technische Universität Darmstadt, Merckstraße 25, Darmstadt, Germany.
*Corresponding author. Email: dragomir.neshev@anu.edu.au

need multiple spatial modes to realize different propagation angles or circularly polarized light, respectively. Here, we demonstrate for the first time selective coupling of modes of different linear polarization to modes of specific polarization and propagation direction in a rib silicon waveguide (see Fig. 1). In this way, we realize a highly compact integrated device for polarization and mode (de)multiplexing, which could enable a significant increase of channel capacity in integrated optical communication systems. Although we specifically investigate coupling from free space to a waveguide, our concept can be readily applied to the coupling between two waveguides.

Strikingly, although most integrated optical applications require the manipulation of high-frequency modulated telecom data streams, the application of waveguide integrated nanoantennas for these applications has not yet been demonstrated. Using the developed nanoantenna, we here show experimentally that on-chip nanoantennas with complex functionality do not affect the quality of typical telecom data streams with 10-GHz signal modulation. The measured low distortion to the transmitted data streams instantly enables applications in integrated data transmission systems, where polarization multiplexing and coherent polarization-state detection are used to improve the data transmission capacity (43, 44). Our results show that plasmonic nanoantennas can preserve their functionalities when transferred onto a dielectric waveguide platform and that they are very well suitable for high-frequency on-chip signal processing at telecommunication wavelengths. This makes them a plasmonic key element for on-chip optical data processing that can also be used as a functional link between on- and off-chip optical signals.

RESULTS
Antenna design
Because we aim to couple light from free space to specific modes of a dielectric waveguide (Fig. 1), we need to develop a nanoantenna that couples each of the two polarization modes of free space to one of the four possible waveguide modes [forward/backward-propagating and transverse electric (TE)/transverse magnetic (TM)–polarized]. In the design process, we will optimize two quantities, namely, the polarization selectivity and the directivity of our nanoantennas. The polarization selectivity is defined as the ratio of the optical powers coupled to the waveguide mode with the desired polarization and coupled to the mode with the other polarization. Similarly, the directivity is defined as the ratio of the powers coupled in both propagation directions.
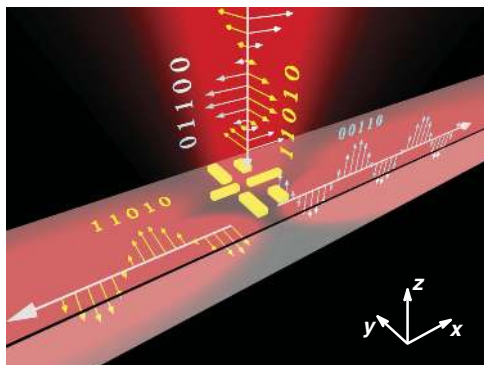

Fig. 1. Scheme of a waveguide-integrated plasmonic nanoantenna for mode-selective polarization (de)multiplexing. The device couples light of orthogonal polarizations into different directions and modes of the underlying silicon waveguide.

In the first step, we numerically design a polarization-sensitive gold nanoantenna that can couple horizontally (x-) polarized incident light from free space to the TM mode of the underlying silicon waveguide (Fig. 2A) and a second one that couples vertically (y-) polarized incident light to the TE mode (Fig. 2B). In addition to this, the two antenna designs should support unidirectional waveguide coupling to selectively guide the light into a specific direction. The TM antenna shown in Fig. 2A consists of two horizontally aligned (along the x axis) gold nanorods of different lengths ($l_{TM1} = 190$ nm and $l_{TM2} = 140$ nm; $w_{TM} = 40$ nm; $h_{TM} = 40$ nm) that are displaced by a center-to-center distance of 195 nm with respect to each other in the x direction. Because of the orientation of the two elements, the TM antenna can only be excited by horizontally polarized light. The radiation of both elements is only coupled to the TM mode of the waveguide, and the polarization selectivity for the TM antenna is 292. The two gold nanorods of different sizes have different resonance wavelengths. Consequently, for in-phase excitation of the two elements, they will resonate with a particular phase offset, which depends on their length difference and the excitation wavelength. The larger element has the larger phase delay with respect to the driving field because it has the lower resonance frequency. Consequently, for light scattered by the two elements in the direction of the larger element, the phase offset between the two elements is reduced by the propagation phase acquired by light traveling from the smaller element to the larger one, thus leading to constructive interference. In contrast, in the opposite direction, the pickup of propagation phase increases the phase mismatch for light scattered by the two elements, resulting in destructive interference. Therefore, the TM antenna enables unidirectional waveguide coupling of horizontally polarized incident light to the right-hand side and into the TM mode of the waveguide with a directivity of 45. Following the same reasoning, the TE antenna (Fig. 2B) enables unidirectional waveguide coupling of vertically polarized incident light to the left-hand side and into the TE mode of the waveguide. However, in contrast to the TM antenna, the TE antenna is composed of two vertically aligned (y direction) nanorods ($l_{TE1} = 180$ nm and $l_{TE2} = 144$ nm; $w_{TE} = 60$ nm; $h_{TE} = 40$ nm that are displaced by a center-to-center distance of 130 nm with respect to each other in the x direction. The center-to-center distance between two pairs of nanorods in the TE antenna is 260 nm in the y direction. The mode selectivity value for the TE antenna is 53, and its directivity is again 45.

Having established these basic nanoantenna elements, which allow for mode-selective and directional waveguide coupling, we now use this toolbox to design an integrated plasmonic nanoantenna device that allows for on-chip polarization (de)multiplexing. To achieve a clear separation of the polarization-encoded optical signals, we take the above-mentioned TM and TE antennas, which support directional waveguide coupling in opposite waveguide directions, and combine them in one nanoantenna design, as shown in Fig. 3A. The combined nanoantenna then couples horizontal polarization (linear x polarization) to the right-hand side into the TM mode and vertically polarized light (linear y polarization) to the left-hand side into the TE mode (Fig. 3B) of the waveguide with a directivity of approximately 20 toward the left and approximately 55 toward the right side, respectively, at 1550-nm wavelength (Fig. 3C). The directivity shows a resonance at 1550 nm, with a full-width-at-half-maximum width of around 50 nm. This bandwidth is large enough to cover the C telecommunication band used in commercial systems. The coupling efficiency in our simulation was 4% (5%) for coupling to the TM (TE) waveguide modes. Here, we focused on optimizing the directivity and did not aim to increase the efficiency. In all calculations, the silicon waveguide has a height of
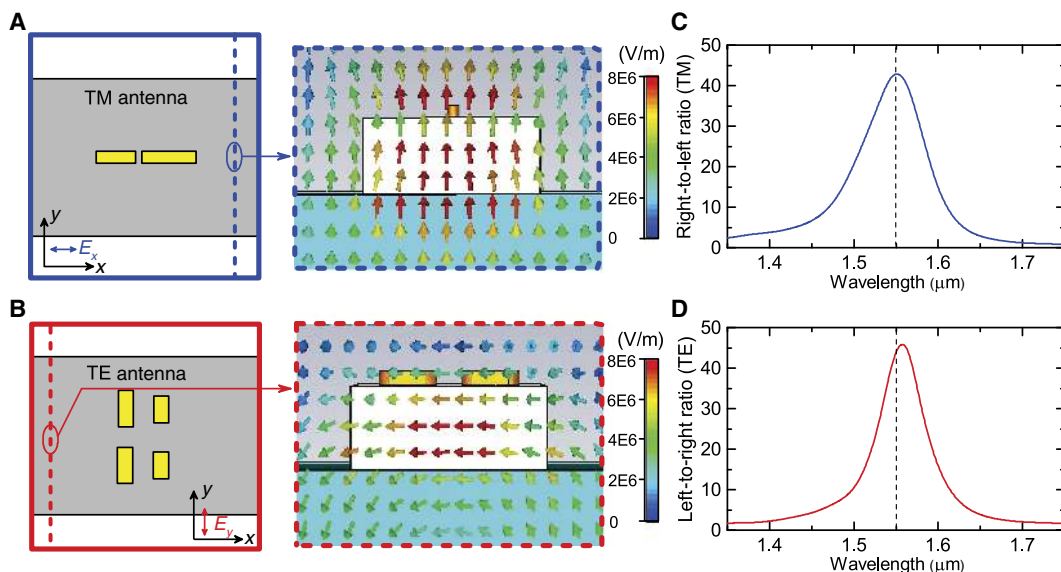
Fig. 2. (A) Numerical design of the nanoantenna coupling *x*-polarized light into the TM mode of the waveguide to the right (TM antenna). The electric field distribution (color-coded arrows) in a cutting plane on the right-hand side of the nanoantenna (blue dashed line) shows that the light is coupled to the TM mode. **(B)** Corresponding design of the TE antenna coupling light to the left-hand side into the TE mode. **(C and D)** Spectrally resolved directivities of the TM antenna coupling to the right and the TM antenna coupling to the left, respectively.
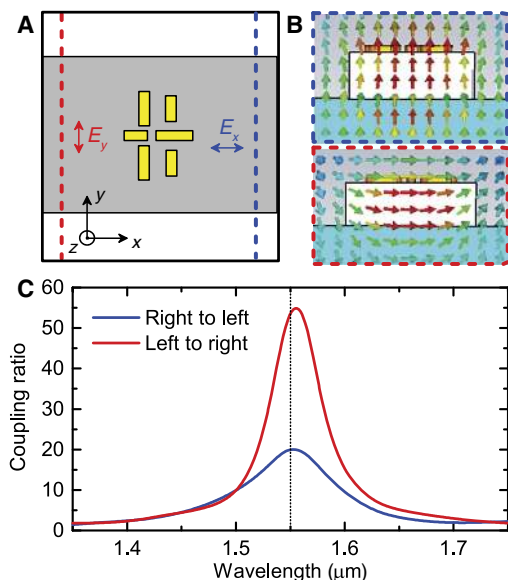
Fig. 3. (A) Design of the combined TE-TM nanoantenna coupling *x*-polarized light to the right (blue dashed line) into the TM mode and *y*-polarized light to the left (red dashed line) into the TE mode of the waveguide. **(B)** Corresponding electric field plots. **(C)** Right-to-left (left-to-right) ratio for directional coupling *x*-polarized (*y*-polarized) incident light with a maximum at around 1550-nm wavelength.

220 nm and a width of 600 nm. The whole device is embedded in an effective medium with a refractive index of $n = 1.46$, corresponding to the poly(methyl methacrylate) (PMMA) cladding layer in the experiment.

We note that, in addition to the polarization-demultiplexing functionality of the combined nanoantenna for free-space excitation, this design can also be used as a waveguide-to-waveguide interconnect (*41*). In this case, the device acts as a (TE-TM) mode (de)multiplexer,

that is, separating information encoded in different waveguide modes. Hence, our nanoantenna can serve both as an ultra-compact bridge between free-space and on-chip photonic circuitry and as an integrated waveguide interconnect.

Polarization and mode selectivities

In the next step, we fabricate all three nanoantennas on a silicon waveguide and investigate their directional coupling properties. To demonstrate the corresponding functionalities of the three integrated nanoantennas, in the following, we will provide evidence for the key elements of our devices—the directional waveguide coupling, the polarization-dependent selective mode coupling, and the compatibility with high-frequency modulation. To do this, we fabricate two nominally identical sample batches. In the first measurement, we detect the radiation that is coupled to the respective waveguide directions for the two orthogonal linear polarizations of the incident light. For this purpose, small gold gratings are processed onto the waveguides of one sample in a distance of approximately 10 μm to the left and to the right of the nanoantennas (see Fig. 4A). By imaging the light that is coupled out by the gratings with an InGaAs charge-coupled device (CCD) camera, we can estimate the directivity of the three antennas depending on the polarization of the incident light (see Fig. 4, B to D) by optimized gratings, which has a similar diffraction response both for the TM and TE modes. Our measurements shown in Fig. 4B (4C) confirm that the TM (TE) antenna couples horizontally (vertically) polarized light to the right-hand (left-hand) side of the waveguide, with maximum directivity toward the left (right) of 4.0 (3.7). Figure 4D shows the results for the combined mode–demultiplexing nanoantenna and experimentally confirms the polarization-demultiplexing functionality; in particular, it shows that, for horizontal polarization, the incident light is coupled to the right, and for vertical polarization, the incident light is coupled to the left. The measured directivities for horizontal and vertical polarization are around 3.3 and 3.7, respectively. The experimentally obtained values
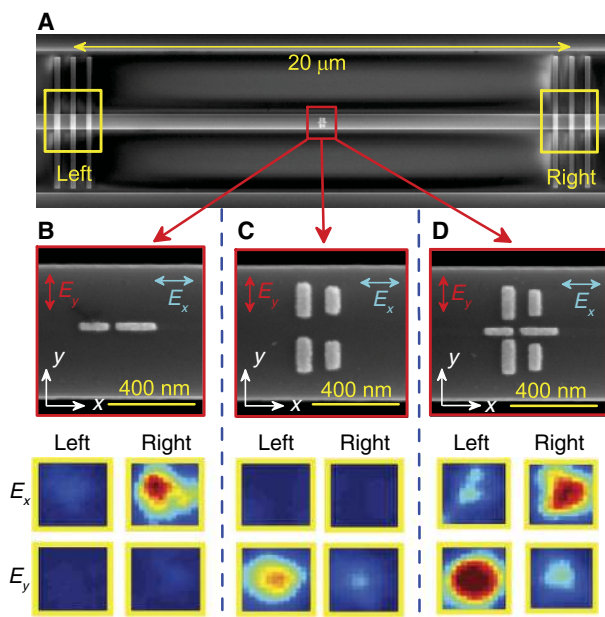
Fig. 4. (**A**) Scanning electron microscope (SEM) images of a setup configuration for measuring the coupling ratios of the three nanoantennas shown in (**B**) (TM antenna), (**C**) (TE antenna), and (**D**) (TE-TM antenna). The nanoantennas are placed in the center (red square) between two gold gratings that are used as output ports (yellow squares) to detect the radiation coupled to the right-hand side and to the left-hand side of the waveguide. (B to D) SEM images (top row) of the fabricated antennas and the intensity plots at the left and right output ports detected on the infrared (IR) camera (second row) for x and y polarization of the incident light at 1550-nm wavelength.

Fig. 5. (**A**) Detected light intensity at the left end of the (cleaved) waveguide with the TE antenna in the center for different polarization angles of the incident light (also indicated as green arrows for the main polarization directions). The light intensity in the TE mode and the TM mode of the waveguide is separated by a polarizing beam splitter in the detection part of the setup and plotted in red and blue, respectively. For vertical polarization at 90° (corresponding to y polarization), the intensity in the TE mode is at its maximum. (**B**) Detected light intensity at the right end of the (cleaved) waveguide, with the TM antenna on top. Here, we find an intensity maximum for horizontal polarization (0/180°, x polarization) in the TM mode. (**C** and **D**) Corresponding plots measured at both the left (C) and the right (D) waveguide end for the combined TE-TM antenna, confirming the coupling of y-polarized (x-polarized) light to the TE mode (TM mode) to the left (right).

are somewhat smaller than expected from the simulations. This is due to small fabrication inaccuracies, which inhibit the needed destructive interference in the direction where propagation should be suppressed.

The same measurement arrangement was used to measure the coupling efficiencies, that is, the ratio of detected light intensity through the waveguides and the intensity of the incident light beam, and we found values of 3.6% (3%) for coupling to the TM (TE) waveguide modes, respectively. Notably, these efficiencies are achieved for nanoantennas that are a factor of 3 smaller than the wavelength of the incident light and, therefore, a factor of 3 smaller than the diffraction-limited spot size. As a result, only a small fraction of the incident light interacts with the antenna, resulting in a limited coupling efficiency.

In the second experiment, we provide evidence for the mode-selective coupling properties of the integrated nanoantennas. To this end, we use the second set of nominally identical samples but without the gratings on top of the waveguide. We image the waveguide facet on either side of the cleaved sample with a CCD camera and use a polarizing beam splitter to discriminate between the TE and the TM mode of the waveguide. We then detect the emerging light intensity in both waveguide modes depending on the polarization of light incident on the nanoantenna in the middle of the waveguide. These results are shown in Fig. 5. For the TM (TE) antenna, we detect the signal on the right (left) waveguide facet, whereas for the combined antenna, we measure on both sides. Our results presented in Fig. 5A (5B) show that for the TE (TM) antenna, vertical (horizontal) polarization is coupled to the TE (TM) mode of the waveguide and is propagating in the directions expected from the measurements presented in Fig. 4. For the combined nanoantenna, we measured the polarization-dependent light intensity for both modes
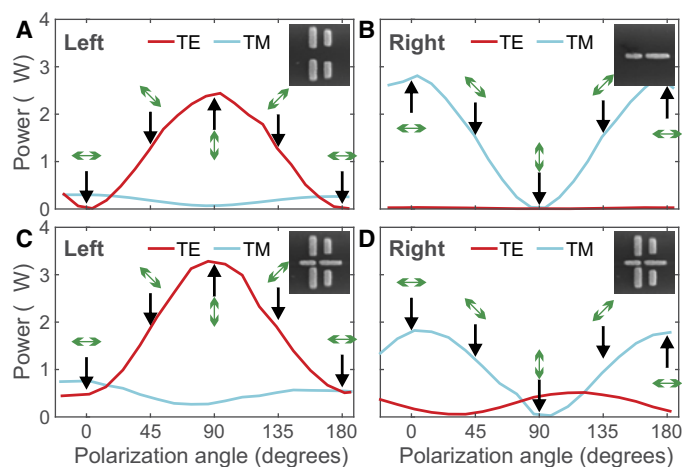
and both directions. These results are plotted in Fig. 5 (C and D) and show that the vertical polarization of light is coupled to the left in the TE mode and the horizontal polarization is coupled to the right in the TM mode, respectively.

High-speed signal transmission

Having experimentally demonstrated the mode-selective directional waveguide coupling and the polarization-(de)multiplexing capabilities of our waveguide-integrated nanoantenna, we finally investigate the suitability of our integrated plasmonic system for high–bit rate signal transmission, which is required for telecommunication applications. Although fundamentally the maximum modulation frequency is only limited by the plasmon decay time, which is on the order of tens of femtoseconds (corresponding to terahertz modulation frequencies), we want to explore the performance of our devices in terms of signal quality at 10-GHz modulation frequency. The most important characteristic of a digital transmission link with this regard is the bit error rate (BER) of the system, that is, the probability of incorrect bit identification by a decision circuit. Usually, BERs of 10^{-12} to 10^{-15} are achieved for telecommunication links after forward-error correction (*45*). To characterize the components used in a transmission link, the BER penalty is used, describing the change in the BER introduced by the component under test, when compared to an element that introduces a similar amount of optical loss without distorting the signal (*46*).

To determine the effect of our nanoantenna on the BER of a typical telecommunication signal, we set up a transmission link for an optical signal modulated with 10 GHz generated by a standard pseudorandom bit sequence generator (PRBS). This optical input is coupled to the TM antenna, which exhibits the best polarization selectivity, collected from the output of the waveguide, reamplified, and then analyzed using a

sampling oscilloscope. With this setup, we measure the characteristic eye diagram of the received signal (see Fig. 6A) and extract the probability density function for the detection of logical ones and logical zeros (Fig. 6B) for several input powers. The evaluation of the latter finally gives us the decision threshold x_0 and the BER of the system under the current conditions (46), plotted with the red dots in Fig. 6A as a function of the received power. To fully quantify the influence of the nanoantenna on the transmission link, we compare the BER of the signal transmitted through the sample with the signal transmitted through an optical attenuator with the same transmission. The measured BERs for this case are plotted with black squares in Fig. 6C. From these results, we can see that the plasmonic nanoantenna does not introduce any noticeable BER penalty into the transmission link and hence is well suited to be used for telecommunication applications, such as coherent detection, which requires splitting the signal in two polarizations before mixing these with the local oscillators.

DISCUSSION

In conclusion, we have designed and characterized plasmonic nano-antennas integrated on silicon waveguides that allow for polarization-dependent, mode-selective, and directional waveguide coupling at 1550-nm wavelength. We experimentally confirm these properties and, furthermore, demonstrate by analyzing an optical signal with 10-GHz modulation frequency that the waveguide-integrated nano-antennas are suitable for on-chip telecommunication applications because of their low BER penalty. Using these ultra-compact hybridized antennas, we finally realize an on-chip polarization-(de)multiplexing device that can be deployed either as a functional link between free-space

signals and on-chip optical circuitry or as a functional element connecting two optical waveguides. In the latter case, the integrated nanoantenna can serve as a mode demultiplexer. Hence, our polarization- and mode-(de)multiplexing plasmonic nanoantennas provide a set of ultra-compact integrated functional elements for on-chip optical circuitry. However, to realize complex circuits involving many plasmonic nanoan-tennas, the efficiencies of these devices have to be increased. This can be achieved by optimizing the antenna shape so that the mode overlap between the localized resonance modes and the waveguide modes is increased while maintaining the high directionality. Such multidimensional optimization of nano-optic elements was already demonstrated for other applications (47, 48). This optimized device could also be applied for future applications in integrated quantum optics, where polarization is an important degree of freedom used to create entanglement (34).

MATERIALS AND METHODS
Numerical calculations
For the numerical calculations, we used the finite element frequency domain solver of the software package CST Microwave Studio. We first calculated and optimized the properties of a single-mode waveguide made from silicon, resulting in a waveguide width of 600 nm and a height of 220 nm. The refractive index of silicon was assumed to be 3.5 at 1550-nm wavelength. The waveguide was placed on a glass substrate with a refractive index of 1.45 and embedded in a PMMA cladding layer with a refractive index of 1.46. This configuration then resulted in an effective index for the TE and the TM mode of 2.98 and 1.99, respectively. In the second step, we used two orthogonal linear polarizations of light to excite the antennas, which were placed on top of the silicon waveguides, and optimized the nanoantenna dimensions to achieve optimum directional coupling ratios, mode selectivity values, and coupling efficiencies. Last, we designed the gold gratings that enable the detection of the coupled light for the front-to-back ratio and the directional coupling measurements. For this purpose, we used the averaged effective wavelength at 1550 nm of the TE and the TM mode as the grating period, which is about 650 nm. The width of each gold stripe is 200 nm, and the thickness is 40 nm.

Sample fabrication
To fabricate nanoantenna waveguide samples, we performed a three-step electron-beam lithography (EBL) process on a silicon on insulator (SOI) wafer (220-nm top silicon thickness, 2-μm buried oxide thickness). In the first step, we fabricated the single-mode silicon waveguides. First, we spin-coated ZEP520A resist and then performed FBMS (fixed-beam moving-stage) mode EBL. After the electron beam exposure, development was performed using cold ZEP developer, followed by a rinse in isopropanol. Using the developed resist as an etch mask, we applied the ICP (inductively coupled plasma) etching process using CHF_3 and SF_6 as etching gases. The remaining resist was removed by using oxygen plasma. In the second EBL step, we fabricated alignment markers around each of the waveguides. Therefore, we spin-coated the PMMA950 resist. After electron beam exposure and consecutive development of the resist, we deposited a 30-nm Au film by using electron-beam evaporation and performed a lift-off procedure in hot acetone. In the third EBL step, we repeated this procedure to fabricate the gold nanoantennas on top of the waveguide. To place them with nanometer precision on top, we used the alignment markers from the last fabrication step. Last, we spin-coated a layer of PMMA950A as a cladding layer for the antenna waveguide system.
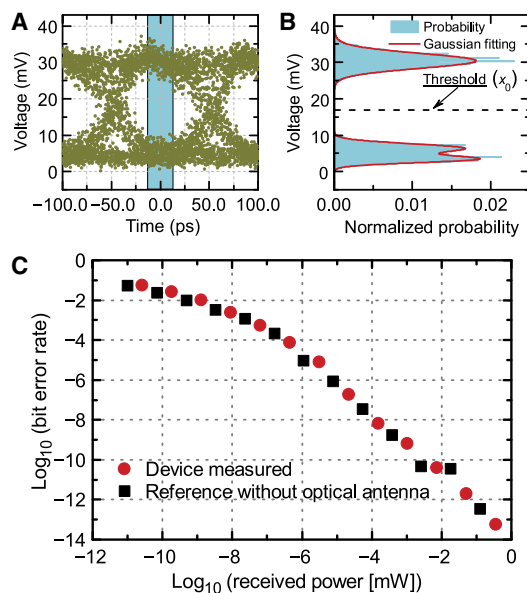

Fig. 6. (A) Measured eye diagram for the TM antenna at 10-GHz modulation frequency. The blue-shaded area is used for the statistical evaluation of the signal and the calculation of the BER. **(B)** Probability density function for the detection of a logical one and zero and the Gaussian fitting used to determine the decision threshold x_0 and to calculate the BER. **(C)** Evaluated BER of the transmission link with the nanoantenna (red dots) and without antenna (black squares) for a series of received powers at the detector. As seen, the two data series are almost identical; therefore, the measured BER is not influenced by the antenna.

High-frequency measurement setup

In the optical modulation tests, a typical prototype of a fiber optic tele-communication line, as described by Kharitonov et al. (46), was used. The optical signal was generated from the transmitter part, and the signal was guided by an optical setup to the sample. Last, the output signal from the sample was collected and analyzed in the receiver part. In the transmitter part, we used an Anritsu MP1701A pulse pattern generator to generate a PRBS electrical signal, which drives a JDS Uniphase Mach-Zehnder modulator to get an optical PRBS. The resulting modulated optical signals were amplified by a Manlight erbium-doped fiber amplifier (EDFA) to a power of 100 mW. Before exciting the plasmonic nanoantennas on the waveguides, we introduced a linear polarizer and a half-wave plate to adjust the polarization state of incident light. In the receiver part, we used a lensed fiber to collect light emerging at the end of the silicon waveguide. The light from the lensed fiber passed through another EDFA to amplify the optical signal from the device output. To control the received power, the amplified signal was then again attenuated by a variable optical attenuator. The optical signals were converted into electronic signals with an HP 11982A Lightwave converter. Last, the electronic signal was detected and analyzed by an HP 83480A digital communications analyzer.

Coupling ratio measurement setup

The nanoantenna directional coupling measurements were performed using a self-made reflection setup. In this setup, a 1550-nm continuous-wave laser was focused on the nanoantenna with a Mitutoyo 100X NIR objective (numerical aperture, 0.7). Light outcoupled from the waveguide by the gratings on either side of the nanoantennas was collected with the same objective. A beamsplitter then deflected the reflected light onto a Xenics InGaAs IR camera. The polarization of the incident light was controlled by a half-wave plate positioned after the laser beam collimator.

REFERENCES AND NOTES

1. L. Novotny, N. van Hulst, Antennas for light. Nat. Photonics 5, 83–90 (2011).
2. D. Dregely, R. Taubert, J. Dorfmüller, R. Vogelgesang, K. Kern, H. Giessen, 3D optical Yagi–Uda nanoantenna array. Nat. Commun. 2, 267 (2011).
3. I. Staude, I. S. Maksymov, M. Decker, A. E. Miroshnichenko, D. N. Neshev, C. Jagadish, Y. S. Kivshar, Broadband scattering by tapered nanoantennas. Phys. Stat. Solidi 6, 466–468 (2012).
4. D. Vercruysse, Y. Sonnefraud, N. Verellen, F. B. Fuchs, G. Di Martino, L. Lagae, V. V. Moshchalkov, S. A. Maier, P. Van Dorpe, Unidirectional side scattering of light by a single-element nanoantenna. Nano Lett. 13, 3843–3849 (2013).
5. A. G. Curto, G. Volpe, T. H. Taminiau, M. P. Kreuzer, R. Quidant, N. F. van Hulst, Unidirectional emission of a quantum dot coupled to a nanoantenna. Science 329, 930–933 (2010).
6. T. Kosako, Y. Kadoya, H. F. Hofmann, Directional control of light by a nano-optical yagi–uda antenna. Nat. Photonics 4, 312–315 (2010).
7. I. M. Hancu, A. G. Curto, M. Castro-López, M. Kuttge, N. F. van Hulst, Multipolar interference for directed light emission. Nano Lett. 14, 166–171 (2013).
8. Z. Li, T. Shegai, G. Haran, H. Xu, Multiple-particle nanoantennas for enormous enhancement and polarization control of light emission. ACS Nano 3, 637–642 (2009).
9. S. S. Kruk, M. Decker, I. Staude, S. Schlecht, M. Greppmair, D. N. Neshev, Y. S. Kivshar, Spin-polarized photon emission by resonant multipolar nanoantennas. ACS Photon. 1, 1218–1223 (2014).
10. S. Kühn, U. Håkanson, L. Rogobete, V. Sandoghdar, Enhancement of single-molecule fluorescence using a gold nanoparticle as an optical nanoantenna. Phys. Rev. Lett. 97, 017402 (2006).
11. A. Kinkhabwala, Z. Yu, S. Fan, Y. Avlasevich, K. Müllen, W. E. Moerner, Large single-molecule fluorescence enhancements produced by a bowtie nanoantenna. Nat. Photonics 3, 654–657 (2009).
12. M. Decker, I. Staude, I. I. Shishkin, K. B. Samusev, P. Parkinson, V. K. A. Sreenivasan, A. Minovich, A. E. Miroshnichenko, A. Zvyagin, C. Jagadish, D. N. Neshev, Y. S. Kivshar, Dual-channel spontaneous emission of quantum dots in magnetic metamaterials. Nat. Commun. 4, 2949 (2013).
13. D. K. Gramotnev, S. I. Bozhevolnyi, Plasmonics beyond the diffraction limit. Nat. Photonics 4, 83–91 (2010).
14. R. Zia, J. A. Schuller, A. Chandran, M. L. Brongersma, Plasmonics: The next chip-scale technology. Mater. Today 9, 20–27 (2006).
15. G. Konstantatos, E. H. Sargent, Nanostructured materials for photon detection. Nat. Nanotechnol. 5, 391–400 (2010).
16. M. W. Knight, H. Sobhani, P. Nordlander, N. J. Halas, Photodetection with active optical antennas. Science 332, 702–704 (2011).
17. I. Goykhman, B. Desiatov, J. Khurgin, J. Shappir, U. Levy, Locally oxidized silicon surface-plasmon Schottky detector for telecom regime. Nano Lett. 11, 2219–2224 (2011).
18. A. Sobhani, M. W. Knight, Y. Wang, B. Zheng, N. S. King, L. V. Brown, Z. Fang, P. Nordlander, N. J. Halas, Narrowband photodetection in the near-infrared with a plasmon-induced hot electron device. Nat. Commun. 4, 1643 (2013).
19. H. Chalabi, D. Schoen, M. L. Brongersma, Hot-electron photodetection with a plasmonic nanostripe antenna. Nano Lett. 14, 1374–1380 (2014).
20. A. Melikyan, L. Alloatti, A. Muslija, D. Hillerkuss, P. C. Schindler, J. Li, R. Palmer, D. Korn, S. Muehlbrandt, D. Van Thourhout, B. Chen, R. Dinu, M. Sommer, C. Koos, M. Kohl, W. Freude, J. Leuthold, High-speed plasmonic phase modulators. Nat. Photonics 8, 229–233 (2014).
21. W. Cai, J. S. White, M. L. Brongersma, Compact, high-speed and power-efficient electrooptic plasmonic modulators. Nano Lett. 9, 4403–4411 (2009).
22. P. Berini, I. De Leon, Surface plasmon–polariton amplifiers and lasers. Nat. Photonics 6, 16–24 (2012).
23. C. Zhao, J. Zhang, Plasmonic demultiplexer and guiding. ACS Nano 4, 6433–6438 (2010).
24. A. Minovich, A. E. Klein, N. Janunts, T. Pertsch, D. N. Neshev, Y. S. Kivshar, Generation and near-field imaging of airy surface plasmons. Phys. Rev. Lett. 107, 116802 (2011).
25. J. S. Q. Liu, R. A. Pala, F. Afshinmanesh, W. Cai, M. L. Brongersma, A submicron plasmonic dichroic splitter. Nat. Commun. 2, 525 (2011).
26. T. Tanemura, K. C. Balram, D.-S. Ly-Gagnon, P. Wahl, J. S. White, M. L. Brongersma, D. A. B. Miller, Multiple-wavelength focusing of surface plasmons with a nonperiodic nanoslit coupler. Nano Lett. 11, 2693–2698 (2011).
27. L. Li, T. Li, S. Wang, S. Zhu, X. Zhang, Broad band focusing and demultiplexing of in-plane propagating surface plasmons. Nano Lett. 11, 4357–4361 (2011).
28. C. Zhao, J. Zhang, Y. Liu, Light manipulation with encoded plasmonic nanostructures. EPJ Appl. Metamater. 1, 6 (2014).
29. M. Février, P. Gogol, A. Aassime, R. Mégy, C. Delacour, A. Chelnokov, A. Apuzzo, S. Blaize, J.-M. Lourtioz, B. Dagens, Giant coupling effect between metal nanoparticle chain and optical waveguide. Nano Lett. 12, 1032–1037 (2012).
30. M. Février, P. Gogol, G. Barbillon, A. Aassime, R. Mégy, B. Bartenlian, J.-M. Lourtioz, B. Dagens, Integration of short gold nanoparticles chain on SOI waveguide toward compact integrated bio-sensors. Opt. Express 20, 17402–17410 (2012).
31. M. Février, P. Gogol, J.-M. Lourtioz, B. Dagens, Metallic nanoparticle chains on dielectric waveguides: Coupled and uncoupled situations compared. Opt. Express 21, 24504–24513 (2013).
32. M. Chamanzar, Z. Xia, S. Yegnanarayanan, A. Adibi, Hybrid integrated plasmonic-photonic waveguides for on-chip localized surface plasmon resonance (LSPR) sensing and spectroscopy. Opt. Express 21, 32086–32098 (2013).
33. F. Peyskens, A. Z. Subramanian, P. Neutens, A. Dhakal, P. Van Dorpe, N. Le Thomas, R. Baets, Bright and dark plasmon resonances of nanoplasmonic antennas evanescently coupled with a silicon nitride waveguide. Opt. Express 23, 3088–3101 (2015).
34. J. Wang, D. Bonneau, M. Villa, J. W. Silverstone, R. Santagati, S. Miki, T. Yamashita, M. Fujiwara, M. Sasaki, H. Terai, M. G. Tanner, C. M. Natarajan, R. H. Hadfield, J. L. O'Brien, M. G. Thompson, Chip-to-chip quantum photonic interconnect by path-polarization interconversion. Optica 3, 407–413 (2016).
35. M. Dakss, L. Kuhn, P. F. Heidrich, B. A. Scott, Grating coupler for efficient excitation of optical guided waves in thin films. Appl. Phys. Lett. 16, 523–525 (1970).
36. F. Bernal Arango, A. Kwadrin, A. F. Koenderink, Plasmonic antennas hybridized with dielectric waveguides. ACS Nano 6, 10156–10167 (2012).
37. C. T. DeRose, R. D. Kekatpure, D. C. Trotter, A. Starbuck, J. R. Wendt, A. Yaacobi, M. R. Watts, U. Chettiar, N. Engheta, P. S. Davids, Electronically controlled optical beam-steering by an active phased array of metallic nanoantennas. Opt. Express 21, 5198–5208 (2013).
38. F. J. Rodríguez-Fortuño, G. Marino, P. Ginzburg, D. O'Connor, A. Martínez, G. A. Wurtz, A. V. Zayats, Near-field interference for the unidirectional excitation of electromagnetic guided modes. Science 340, 328–330 (2013).
39. J. Petersen, J. Volz, A. Rauschenbeutel, Chiral nanophotonic waveguide interface based on spin-orbit interaction of light. Science 346, 67–71 (2014).
40. T. P. H. Sidiropoulos, M. P. Nielsen, T. R. Roschuk, A. V. Zayats, S. A. Maier, R. F. Oulton, Compact optical antenna coupler for silicon photonics characterized by third-harmonic generation. ACS Photon. 1, 912–916 (2014).
41. R. Guo, M. Decker, I. Staude, D. N. Neshev, Y. S. Kivshar, Bidirectional waveguide coupling with plasmonic fano nanoantennas. Appl. Phys. Lett. 105, 053114 (2014).

42. R. Guo, M. Decker, F. Setzpfandt, I. Staude, D. N. Neshev, Y. S. Kivshar, Plasmonic fano nanoantennas for on-chip separation of wavelength-encoded optical signals. *Nano Lett.* **15**, 3324–3328 (2015).

43. C. R. S. Fludger, T. Duthel, D. van den Borne, C. Schulien, E.-D. Schmidt, T. Wuth, J. Geyer, E. De Man, G.-D. Khoe, H. de Waardt, Coherent equalization and POLMUX-RZ-DQPSK for robust 100-GE transmission. *J. Lightw. Technol.* **26**, 64–72 (2008).

44. E. Ip, A. P. T. Lau, D. J. F. Barros, J. M. Kahn, Coherent detection in optical fiber systems. *Opt. Express* **16**, 753–791 (2008).

45. I. P. Kaminow, T. Li, *Optical Fiber Telecommunications IV-A, Volume A: Components* (Academic Press, 2002).

46. S. Kharitonov, R. Kiselev, A. Kumar, I. F. de Jáuregui Ruiz, X. Shi, K. Leósson, T. Pertsch, S. Nolte, S. Bozhevolnyi, A. Chipouline, Data transmission in long-range dielectric-loaded surface plasmon polariton waveguides. *Opt. Express* **22**, 26742–26751 (2014).

47. B. Shen, P. Wang, R. Polson, R. Menon, An integrated-nanophotonics polarization beamsplitter with 2.4 × 2.4 μm^2 footprint. *Nat. Photonics* **9**, 378–382 (2015).

48. P. R. Wiecha, A. Arbouet, C. Girard, A. Lecestre, G. Larrieu, V. Paillard, Evolutionary multi-objective optimization of colour pixels based on dielectric nanoantennas. *Nat. Nanotechnol.* **12**, 163–169 (2016).

Citation: R. Guo, M. Decker, F. Setzpfandt, X. Gai, D.-Y. Choi, R. Kiselev, A. Chipouline, I. Staude, T. Pertsch, D. N. Neshev, Y. S. Kivshar, High–bit rate ultra-compact light routing with mode-selective on-chip nanoantennas. *Sci. Adv.* **3**, e1700007 (2017).

Science Advances

High−bit rate ultra-compact light routing with mode-selective on-chip nanoantennas

Rui Guo, Manuel Decker, Frank Setzpfandt, Xin Gai, Duk-Yong Choi, Roman Kiselev, Arkadi Chipouline, Isabelle Staude, Thomas Pertsch, Dragomir N. Neshev and Yuri S. Kivshar

ARTICLE TOOLS	http://advances.sciencemag.org/content/3/7/e1700007
PERMISSIONS	http://www.sciencemag.org/help/reprints-and-permissions

Use of this article is subject to the Terms of Service